Surface Science 631 (2015) 42–47

Contents lists available at ScienceDirect

Surface Science

journal homepage: www.elsevier.com/locate/susc

First principles Tafel kinetics of methanol oxidation on Pt(111)

Ya-Hui Fang [a,b], Zhi-Pan Liu [b]

[a] School of Chemical Environmental Engineering, Shanghai Institute of Technology, Shanghai 201418, China
[b] Shanghai Key Laboratory of Molecular Catalysis and Innovative Materials, Key Laboratory of Computational Physical Science (Ministry of Education), Department of Chemistry, Fudan University, Shanghai 200433, China

ARTICLE INFO

Available online 29 May 2014

Keywords:
Methanol oxidation
Tafel kinetics
First principles
Periodic continuum solvation model

ABSTRACT

Electrocatalytic methanol oxidation is of fundamental importance in electrochemistry and also a key reaction in direct methanol fuel cell. To resolve the kinetics at the atomic level, this work investigates the potential-dependent reaction kinetics of methanol oxidation on Pt(111) using the first principles periodic continuum solvation model based on modified-Poisson–Boltzmann equation (CM-MPB), focusing on the initial dehydrogenation elementary steps. A theoretical model to predict Tafel kinetics (current vs potential) is established by considering that the rate-determining step of methanol oxidation (to CO) is the first C – H bond breaking ($CH_3OH_{(aq)} \rightarrow CH_2OH^* + H^*$) according to the computed free energy profile. The first C – H bond breaking reaction needs to overcome a large entropy loss during methanol approaching to the surface and replacing the adsorbed water molecules. While no apparent charge transfer is involved in this elementary step, the charge transfer coefficient of the reaction is calculated to be 0.36, an unconventional value for charge transfer reactions, and the Tafel slope is deduced to be 166 mV. The results show that the metal/adsorbate interaction and the solvation environment play important roles on influencing the Tafel kinetics. The knowledge learned from the potential-dependent kinetics of methanol oxidation can be applied in general for understanding the electrocatalytic reactions of organic molecules at the solid–liquid interface.

1. Introduction

The direct methanol fuel cells (DMFCs) are regarded as a key technology for energy storage and conversion, which features methanol oxidation reaction (MOR) on an anode to deliver clean, abundant and reliable energy ($CH_3OH + H_2O \rightarrow CO_2 + 6H^+ + 6e^-$) [1–5]. The state-of-the-art DMFC anode catalysts are generally Pt-based materials [6–9]. Extensive studies on MOR kinetics have been carried out in the past decades [10–17] with the aim to reduce Pt usages (e.g. alloys or dispersing into nanoparticles) while improving CO tolerance [18–21]. It is generally accepted that methanol could be oxidized to CO_2 via a dual-path mechanism [22–24], namely, the indirect pathway via adsorbed CO and the direct one without the participation of CO. In both pathways, the dehydrogenation reactions (either the C – H or O – H bond breaking) are the initiating steps. To date, the major concern in the catalyst design is to maintain the dehydrogenation efficiency of Pt while reducing its CO poisoning.

From the combined chronoamperometry and mathematical simulation [11,23,25], it was regarded that the C – H bond breakage (e.g. $CH_3OH \rightarrow CH_2OH + H^+ + e$) is the rate-determining step. This is supported by some theoretical calculations [26–32]. For example, Greeley et al. have shown that the initial C – H bond breaking is the rate-determining step for methanol decomposition in vacuum. The reaction barrier of the O – H bond breaking (0.64 eV) is higher than that of the C – H bond breaking (0.51 eV) [33,34]. The kinetic data from the experiment has been utilized to construct the current ~ overpotential ($\log(j) \sim \eta$) plot, known as the Tafel plot. The Tafel equation as shown Eq. (1) is a fundamental equation in the kinetics of electrochemistry, which relates the overpotential η with the current density j using the charge transfer coefficient α (i.e. if the rate-determining step involving one electron transfer with the charge transfer coefficient α of ca. 0.5, the Tafel slope 2.3RT/αF should be 118 mV). Interestingly, the measured Tafel slopes of methanol decomposition span in a wide window, from 95 to 440 mV by different experimental groups, e.g. 110 and 95 mV for Pt(554) and Pt(553) [11], 130–140 mV at polycrystalline(pc)-Pt [23] and even ~440 mV at pc-Pt [33]. The large distribution of the Tafel slope obtained from experiment, on the other hand, indicates a complex dehydrogenation kinetics on Pt surfaces, which could be quite sensitive to the catalyst condition and the experimental setups.

$$\eta = a + \frac{2.3RT}{\alpha F}\log(j) \quad (1)$$

Ideally, theoretical kinetic model based on first principles calculations should be utilized to benchmark and rationalize different experimental data, as that was often practiced in heterogeneous catalysis [35,36]. One major concern for current density functional theory (DFT)

E-mail address: zpliu@fudan.edu.cn (Z.-P. Liu).

http://dx.doi.org/10.1016/j.susc.2014.05.014
0039-6028/

calculations is the lack of proper means to simulate accurately the electrochemical conditions, in particular to treat simultaneously the electrochemical potential, the surface charging and the solid–liquid interface. With the advent of the periodic DFT/CM-MPB method developed recently, the potential dependent kinetics of elementary electrocatalytic reactions can now be investigated in one unified theoretical framework. This work represents a latest application of the DFT/CM-MPB [37–39] method for resolving the puzzles on the Tafel kinetics of MOR and for providing insights into the oxidation mechanism of organic molecules on metal at the atomic level. Multiple reaction pathways for methanol decomposition on Pt(111) surface are investigated in detail and the free energy profiles are computed, based on which the potential dependent kinetics model is established and discussed in the context of experimental findings.

2. Methods

All DFT calculations were performed using the SIESTA package with numerical atomic orbital basis sets [40,41] and Troullier–Martins normconserving pseudopotentials [42]. The exchange-correlation functional utilized was at the generalized gradient approximation level, known as GGA-PBE [43]. The optimized double-ζ plus (DZP) polarization basis set was employed. All transition states (TSs) of the catalytic reaction were searched using our recently-developed methods within the Constrained-Broyden scheme [44–46]. For Pt(111), we utilized p(4 × 4) (16 atoms per layer) six-layer slabs with adsorbates on both surfaces, respectively. The Monkhorst_Pack type of k-point sampling with a (2 × 2 × 1) mesh was used in all calculations, and the denser (4 × 4 × 1) k-point mesh was used to further check the convergence of reaction energetics. The other calculation detail is as those described in our previous work [47,48].

The solid/liquid interface is described using the periodic continuum solvation model based on the modified Poisson–Boltzmann equation (CM-MPB), which can take into account the long-range electrostatic interaction due to the solvation of electrolyte [37,48,49]. The DFT/CM-MPB method has been utilized to calculate the electro-photo catalytic reactions at the solid–liquid interfaces [37,38,49], and compute the fundamental properties of metal surfaces in the solution, such as the potential of zero charge and the differential capacitance, where the calculated values show a good agreement with the available experimental data [48]. For strongly polarized molecules at the solid–liquid interface, such as CH_3OH and the related reaction intermediates, we have to further add explicit H_2O molecules as the first solvation shell within the DFT/CM-MPB framework to compute accurately the energetics, i.e. via a hybrid approach with both explicit and implicit solvation to describe the solvation environment.

It should be noted that the current DFT/CM-MPB method is performed on the basis of the constant-charge framework, in which a surface slab at a fixed net charge (q) can be routinely calculated. As there are two surfaces per slab, the surface net charge Q_{net} equals to half of the total net charge q, $Q_{net} = q/2$. The neutralizing charge (−q) is distributed in the vacuum region of the slab following the modified Poisson–Boltzmann equation, mimicking the polarized ionic charge distribution (diffuse layer) in the solution [37]. The constant-charge model in calculation is however not exactly what is operated in the experiment, where the electrode is generally held under a certain potential. We therefore need to convert the kinetic data collected at a certain charge q to that at a certain potential U, which can be summarized briefly as follows.

For an elementary reaction, the free energy barrier $\Delta G_a(q = 0,\theta_i)$ at the potential of zero charge (q = 0) condition can be obtained first using Eq. (2),

$$\Delta G_a(q,\theta_i) = G_{TS}(q,\theta_i) - G_{IS}(q,\theta_i) \quad (2)$$

$$\Delta G_a(U,\theta_i) = \Delta G_a(q,\theta_i)|_{q \Leftrightarrow U} \quad (3)$$

where θ_i indicates the surface phase characterized by a particular local coverage *i* and $G_{TS/IS}$ are the free energies at the TS/IS (IS: initial state). In this work, the coverage of methanol is kept as 0.0625 ML on Pt(111), which corresponds to a typical low coverage condition. This first step (q = 0 calculations) involves the location of the relevant TS and ISs at the charge neutral condition, as is typical in standard periodic DFT packages. Next, one needs to establish the linkage between the charge *q* and the potential *U*. This is done by carrying out a series of calculations with the variable *q* and simultaneously measuring the potential *U* of each *q* state using DFT/CM-MPB. The absolute electrochemical potential of the system (a surface slab) can be measured by computing the work function in the solution and then referring it to the experimental work function of the standard hydrogen electrode (SHE, 4.4–4.8 from experiment; and 4.6 V utilized in this work). By this way, the free energy barrier at a concerned *U* can be finally obtained with Eq. (3). The free energy correction (referring to the standard state) to the DFT/CM-MPB total energy can be derived by using the standard thermodynamic equations (see for example ref. [50]). The constant-charge DFT/CM-MPB method for computing the potential dependent kinetics of electrocatalytic reactions has been utilized to resolve the complex reaction network of hydrogen evolution on Pt and Au surfaces recently [51].

3. Results

3.1. CH_3OH adsorption at the interface

To address the kinetics of MOR, it is essential to understand first how methanol molecule adsorbs at the solid/liquid interface, which is the precursor leading to the methanol oxidation. The possible structures of adsorbed CH_3OH on Pt(111) have been explored by using the hybrid explicit/implicit solvation model. The explicit H_2O molecules (at least two molecules) nearby the methanol are found to be important to obtain accurate energetics.

We identified two of the most stable configurations of CH_3OH on Pt(111), namely, the IS-A and IS-B configurations. These two configurations are shown in Fig. 1. In the IS-A configuration (Fig. 1(a)), the O atom of CH_3OH attaches to a surface Pt atom via a O – Pt bond (2.45 Å) together with another adsorbed water molecule; in the IS-B configuration, CH_3OH is hydrogen-bonded (1.51 Å) with the adsorbed H_2O, having no direct contact with the surface. These two structures are quite close to the bilayer structures for H_2O adsorption on metal surfaces as previously found by theory and experiment [52,53]. This may not be surprising considering that the dominant interaction between molecules is the same, i.e. the hydrogen bonding.

$$\Delta E_{ad} = E^{sol}_{CH_3OH\text{-}H_2O/sur} - E^{sol}_{sur} - E^{sol}_{CH_3OH} - 2E^{sol}_{H_2O} \quad (4)$$

The stability of the CH_3OH–H_2O complexes shown in Fig. 1 can be calculated using Eq. (4) by referring to the individual surface or molecules in the bulk water solution, where E_X^{solv} (X = CH_3OH-H_2O/sur, sur, CH_3OH and H_2O) denotes the total energies calculated from the DFT/CM-MPB for system X. We found that the IS-B configuration (−0.74 eV) is slightly more stable compared to the IS-A adsorption configuration (−0.71 eV) (by 0.03 eV), which suggests that the direct interaction between methanol and Pt(111) surface is weak and can be readily influenced by the solvation environment. We noticed that for the adsorbed CH_3OH–H_2O complex, their H-bonding distances are generally shorter (1.51 Å for the IS-B configuration or 1.68 Å for the IS-A) compared to the CH_3OH–H_2O complex in the bulk solution (1.70 Å). This indicates that the molecules upon adsorption are further polarized by the surface through the metal/molecule covalent bonding, which influences the H-bonding interaction at the solid/liquid interface.

To better understand the adsorption strength of the individual methanol molecule, we also compared the ΔE_{ad} for methanol on Pt(111) in vacuum condition and in the CM-MPB solvation condition

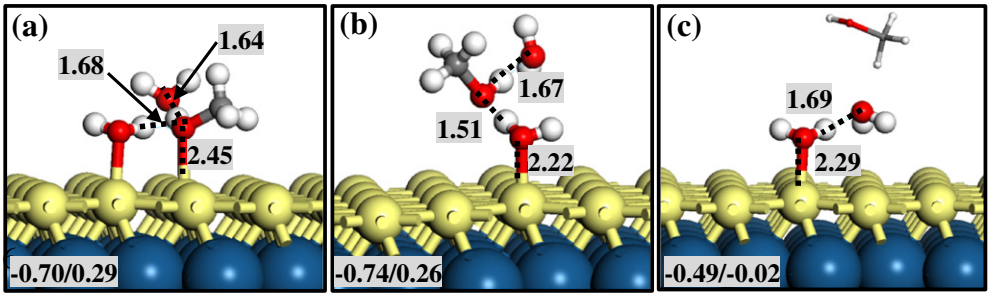

Fig. 1. Possible configurations for methanol at the Pt(111)/water interface. (a) IS-A: methanol and water coadsorption on the surface, (b) IS-B: methanol at the second layer above the surface and (c) IS-C: water-only adsorption on the surface and methanol in the bulk solution. The calculated $\Delta E_{ad}/\Delta G_{ad}$ (eV) at 0.32 V vs. SHE are indicated at the bottom of the figures (as calculated using Eqs. (4)–(5)). The labeled distances are in angstroms. Large ball: Pt atoms. Small yellow ball: surface Pt atoms. Small red ball: O atoms. Small white ball: H atoms.

(with only the implicit solvation, i.e. the long-range polarization). The ΔE_{ad} in vacuum calculated from our DFT is −0.26 eV, which is consistent with that reported by Greeley and Mavrikakis (−0.33 eV) [27]. By switching on the CM-MPB condition, ΔE_{ad} is much reduced to −0.05 eV, which is obviously caused by the change of the reference state (now an individual methanol molecule in CM-MPB solvation condition). These suggest that one individual methanol molecule has only weak interaction with Pt(111): no significant enthalpy preference for transferring methanol from the bulk water solution to the surface.

3.2. Potential-dependent interface composition

To describe the composition of the methanol–water/Pt(111) interface, one needs to compute the potential-dependent free energy diagram for all the possible adsorption configurations for methanol and water on Pt(111). Among various configurations investigated for the interface, three major configurations are of importance and discussed in detail below, including the two methanol adsorption configurations IS-A and IS-B shown above, and a water-only adsorption configuration, termed as IS-C, also shown in Fig. 1. In IS-C, methanol remains in the bulk water solution and the interface contains adsorbed water only, where two water molecules adsorb on Pt(111) in a bilayer-like structure.

In order to compare the free energy of IS-A, IS-B and IS-C, we need to take into account the entropy contribution of the reference molecule in the bulk solution, where a large translation/rotational entropy contribution is present. For methanol solution of 1 M (typically utilized in experiment), we utilize the entropy term of 69.95 J/mol and 159.86 J/mol for water and methanol in bulk solution according to the standard thermodynamic data [54] and thus their entropy term (TS) at 300 K are −0.22 and −0.50 eV, respectively. From these entropy data and the DFT/CM-MPB calculated ΔE_{ad} from Eq. (4), ΔG_{ad} can be calculated according to the fundamental thermodynamic equations [55], where ZPE is the zero-point-energy contribution.

$$\Delta G_{ad} = \Delta E_{ad} + \Delta ZPE - T\Delta S \quad (5)$$

The potential-dependent free energy diagram of the three configurations can then be calculated using the DFT/CM-MPB method and the results are plotted in Fig. 2. The calculated ΔG_{ad} at 0.32 V vs. SHE is also indicated in Fig. 1 (this corresponds to the potential of zero charge (pzc) of Pt(111) from DFT/CM-MPB [48], c.f. the experimental pzc of Pt(111) is 0.2–0.4 V [56]). Generally, with the increase of potential, the free energy of adsorption generally increased (ΔG_{ad} being more negative). This is reasonable considering that the O-ends of H_2O and methanol are electronegative and the O – Pt bonding is enhanced with the increase of potential, as also evident from the computed O – Pt bond length at different potentials. Fig. 2 also shows that at the potentials interested for methanol oxidation, e.g. 0.3 to 0.6 V vs. SHE, the IS-C (the water-only adsorption configuration) are the most stable in free energy, which dominates the Pt/solution interface. It is indicated that methanol oxidation should initiate by methanol coming from the bulk solution, replacing the adsorbed water molecules, a sequence from IS-C to IS-B and to IS-A. IS-A is the precursor for the dehydrogenation reactions.

3.3. Reaction mechanism

Starting from the IS-A configuration, we investigated the reaction channels for methanol decomposition on Pt(111) at the Pt/water interface till the formation of CO. As we are focusing on the Tafel kinetics of MOR at low potentials (0.3 to 0.5 V vs. SHE) in this work and the mechanism of methanol decomposition has been studied previously [27,28], we did not make an attempt to resolve the whole reaction network of methanol oxidation, i.e. to CO_2 formation, which involves the added complexity due to the participation of the oxidative surface species that emerged at high potentials. According to our computed energetics, we found that the initial dehydrogenation steps have the highest free energy barrier in methanol decomposition and the results are elaborated in the following.

The free energy profiles for the two competitive pathways are shown in Fig. 3, together with the representative intermediate structures of the reaction. All the energetics reported in Fig. 3 are collected at the 0.32 V vs. SHE condition (pzc of Pt(111) from DFT/CM-MPB). The first pathway (the C–H pathway) features with the C – H bond breaking of CH_3OH followed by the consecutive dehydrogenation of CH_2OH to CHO; the second pathway (the O–H pathway) involves the O – H bond breaking of CH_3OH. The C–H pathway is the lowest energy pathway of methanol oxidation at the Pt(111)/H_2O interface and the O–H pathway is kinetically unfavorable, which is described in more detail as follows.

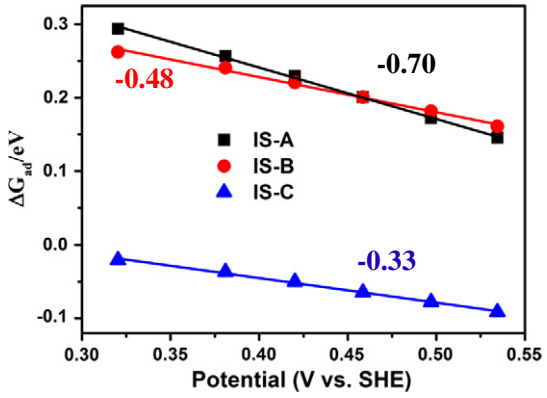

Fig. 2. The potential-dependent free energy diagram of three different configurations of water, methanol on Pt(111). The IS-A, IS-B and IS-C are as shown in Fig. 1. The numbers indicate the slope of the lines by linear fitting.

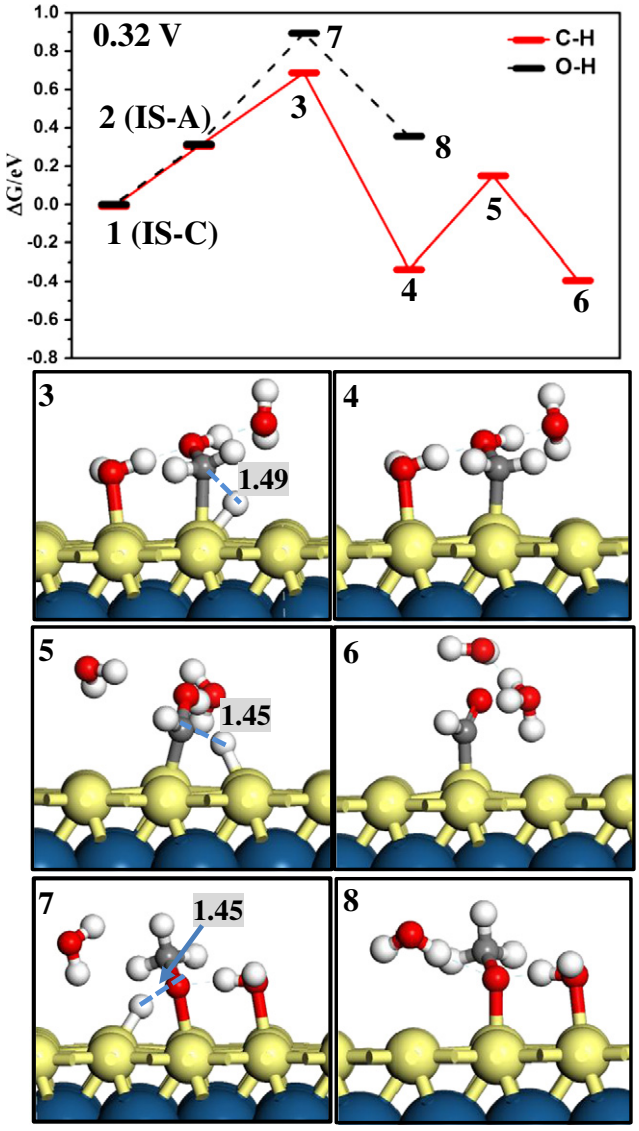

Fig. 3. The free energy profile and the optimized structures of the intermediates of methanol dehydrogenation for the Pt(111)/water interface at 0.32 V. 1 and 2 refer to the IS-C and IS-A, respectively (see Fig. 1); 3, 4, 5 and 6 are the located TSs and FSs in the C–H pathway; 7 and 8 are the located TS and FS in the O–H pathway. The labeled distances are in angstroms. Large ball: Pt atoms. Small yellow ball: surface Pt atoms. Small red ball: O atoms. Small white ball: H atoms.

3.3.1. The C–H pathway

In this pathway, the adsorbed CH_3OH (IS-A, also state **2** in Fig. 3) decomposes by breaking one of its C – H bond. At the transition state (TS), the carbon atom sits on a top site and the dissociating H atom is close to a bridge site (state **3**, Fig. 3), where the dissociating CH bond of CH_3OH is lengthened to 1.49 Å. The free energy barrier is calculated to be 0.38 eV with respect to IS-A (state **2**) and 0.70 eV with respect to the most stable IS-C (also state **1** in Fig. 3). The calculated barrier at the Pt/water interface is larger than the previous DFT calculations in vacuum (0.51 eV) [27]. The final state is an adsorbed CH_2OH fragment (state **4**), while the dissociated H on the surface is unstable on Pt(111) above pzc and can desorb to solution facilely (also see our previous work for detailed energetics [51]). Hereafter only the non-H adsorbates will be discussed.

The next step is the C – H bond breaking of the CH_2OH. At the IS of CH_2OH adsorption (state **4**), CH_2OH sits on a top site and the C-Pt bond distance is 2.09 Å. At least two nearby H_2O molecules are essential as the first solvation shell to stabilize the CH_2OH fragment. In particular, the H-bonding between the H of the adsorbed H_2O and the O of the CH_2OH appears to be strong with the distance being only 1.56 Å. At the TS (state **5**), one C – H bond distance is lengthened to 1.45 Å and the C atom remains on the top site (also see state 5, Fig.3). It is noticed that the first solvation shell changes from the IS to the TS for CH_2OH dehydrogenation. Compared to the IS where two H-bondings with nearby H_2O are present for the adsorbed CH_2OH, only one H-bonding is left at the TS that links the H of hydroxyl in CH_2OH with the nearby O of H_2O. This is obviously due to the fact that at the TS of CH_2OH dissociation, the [CHOH] fragment has a strong acidity at its hydroxyl H, which prefers only the bonding with electronegative species.

3.3.2. The O–H pathway

This pathway is initiated by the cleavage of the hydroxyl group of CH_3OH, which produces an adsorbed methoxyl. The TS (state **7**) is achieved when the OH of CH_3OH passes its H to the neighboring Pt atoms and the O–H distance is lengthened to 1.45 Å, which is also shown in Fig. 3. The free energy barrier is calculated to be 0.58 eV with respect to IS-A and 0.89 eV to the most stable IS-C. At the FS (state **8**), an adsorbed methoxy is formed, which adsorbs at the top site via its O end. It is noticed that the CH_3O fragment is very unstable (0.36 eV) on Pt(111) compared to the CH_2OH fragment. This large difference from thermodynamics has been utilized to explain why the C – H bond breaking of alcohol is generally preferred over the Pt surfaces [27,44,57].

It is of interest to compare our calculated reaction energy with those reported previously, although the current theoretical methods (DFT/CM-MPB) differ from those utilized previously. In this work, we found that the reaction energies are −0.34 and 0.36 eV for the C – H and the O – H bond breaking, respectively. In literatures, the reported values are from −0.1 to −0.4 eV for the C – H bond breaking [27,30,57] and about 0.6–0.7 eV for the O – H bond breaking in the vacuum condition [34]. Using a static water layer model at Pt(111)/water surface, Neurock et al. obtained the reaction energies of −0.78 and −0.04 eV for the C – H and the O – H, respectively [28]. Their results indicate that the presence of water at the interface can dramatically decrease the reaction energy of the dehydrogenation (by better stabilizing the product). Our results are in line with these previous results, showing that the C – H bond breaking is thermodynamically favored and the solvation can influence the thermodynamics markedly.

3.4. Potential ~ barrier relationship and tafel lines

We are now at the position to examine the potential dependent kinetics of the key elementary step in methanol oxidation. From Fig. 3, the first C – H bond breaking is the rate determining step of methanol decomposition and thus should determine the Tafel kinetics of methanol oxidation. By focusing on the C – H bond breaking, we have computed the ΔG_a of the reaction at different potentials using the charged-slab DFT/CM-MPB method. The procedure of using charged-slab DFT/CM-MPB method to compute the Tafel kinetics of electrocatalytic reactions has been detailed in our recent publications [51,58] and also briefly in the Methods section. For comparison, we also calculated the potential ~ barrier relation for the O – H bond breaking. These results are plotted in Fig. 4a.

Fig. 4a shows that the ΔG_a of the first C – H bond breaking decreases linearly with the increase of potential, indicating that the rate for the methanol decomposition increases by elevating potential. By contrast, the ΔG_a of the O – H bond breaking increases slightly with the increase of potential, i.e. at the opposite trend with that of the C – H bond breaking.

In electrochemistry, the Tafel equation (Eq. (1)) that relates the rate of electrochemical reactions with the overpotential η can be rationalized

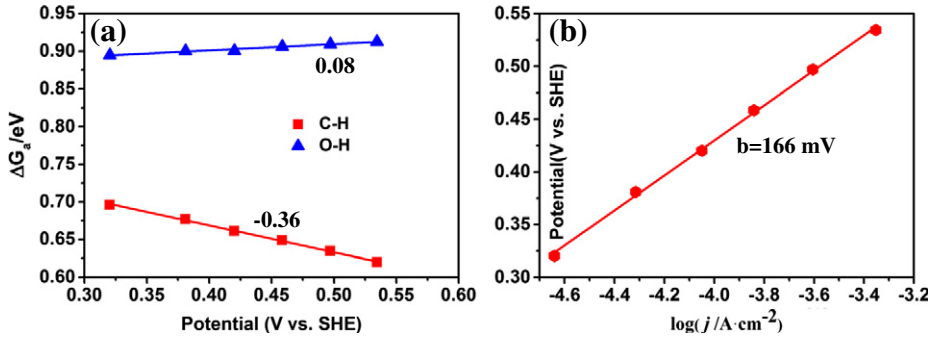

Fig. 4. (a) The plot of the barrier (ΔG_a) against the electrochemical potential plot for the first C – H and O – H bond breaking of methanol on Pt(111). (b) Theoretical Tafel plot (U vs $\log(j)$) for methanol oxidation on Pt(111).

using Eq. (6), which states that the variation of potential influences the free energy barrier.

$$\Delta G_a = \Delta G_a^{\,0} - \alpha F(U - U_0) \tag{6}$$

where ΔG_a^0 is the free energy barrier at a reference potential U_0 and α is the charge transfer coefficient as defined in Tafel equation. Using Eq. (6), we can thus fit the $\Delta G_a \sim U$ relation for the C – H bond and the O – H bond breaking in Fig. 4a. We found that the obtained α value for the C – H bond breaking is −0.36, and that for the O – H bond breaking it is 0.08. The α of the two reactions has the opposite sign, indicating that these two reactions have different redox behaviors. This can be rationalized by considering that these two reactions can be formally written as, $CH_3OH_{(aq)} \rightarrow CH_3O^{*q-} + H^* + q^+$ and $CH_3OH_{(aq)} \rightarrow CH_2OH^{*q+} + H^* + q^-$ (* indicates the adsorption) according to the polarization character of the CH_3O and CH_2OH fragments. Obviously, the increase of potential (via positive surface charging) will favor the C – H bond breaking but hinder the O – H bond breaking.

Importantly, the fitted α values of the dehydrogenation reactions are not 0.5 or 1 as often utilized in electrochemistry for one or two electron transfer reactions. This indicates that the rate determining step of the methanol oxidation cannot be simply considered as a classical one electron transfer reaction. Indeed, according to the IS, TS and FS of the dehydrogenation reaction identified in this work, we can conclude that the C – H (or the O – H) bond breaking reaction is a surface catalyzed elementary reaction involving no apparent charge transfer. In other words, although one H is removed from the CH_3OH molecule, this dissociated H must initially attach to the Pt surface and can only leave the surface as a solvated proton (one electron transfer reaction) after the dehydrogenation reaction (this secondary reaction is a fast step [51]). This could explain why the α value of the dehydrogenation reactions is generally small.

On the other hand, the non-diminishing α value for the dehydrogenation reactions is due to the interfacial dipole change from the IS to the TS. Taking the C–H bond dissociation reaction as the example, we found that the dissociation experiences a remarkable structural change as reflected in the restructuring of the solvation shell. As we have shown in Fig. 2, the IS-C of the methanol dissociation features with the water-only adsorption interface and methanol in the bulk solution. By contrast, at the TS, the C of the methanol has a direct contact with the surface to break its C – H bond. Such changes at the interfacial composition will certainly lead to the change of the interface dipole and thus result in a non-diminishing α.

Finally, based on the potential-dependent kinetic data, it is possible for us to deduce the MOR rate as measured by the current j at low potentials according to microkinetics as expressed in Eq. (7),

$$j = AFS^{-1}N_A{}^{-1}e^{-\Delta G_a(U)/RT}[site] \tag{7}$$

where A is the preexponential factor (it is $kT/h = 6.25 \times 10^{12}\ s^{-1}$ at 300 K); S is the total surface area; [site] is the concentration of the reactive site (ML), N_A is the Avogadro's constant. In computing j, $\Delta G_a(U)$ of the first C – H bond breaking reaction (Fig. 4a) is utilized since this reaction is the rate-determining step; [site] is taken as 0.0625 ML as modeled in this work; the surface area S is $1.097 \times 10^{-14}\ cm^2$ for Pt(111). In Fig. 4b, we plotted the calculated j vs. U for methanol oxidation and the derived theoretical Tafel slope, $b = \partial\eta/\partial\log(j)$, is 166 mV at the potentials investigated.

It is of interest to examine the current kinetics model established based on first principles calculations in the context of previous experimental studies. As for the Tafel slope, the theoretical value 166 mV on Pt(111) is in the range of those reported in the experiment [4,11,23]. It is noticed that the experimental data is generally collected on Pt surfaces containing a large faction of stepped Pt sites, such as polycrystalline Pt. The scattered experimental data on the Tafel slope implies that the Tafel kinetics of methanol oxidation could be influenced markedly by the experimental condition, such as the surface site, the electrolyte and even the methanol concentration. Our results suggest that MOR kinetics is controlled by the first C – H bond breaking step, which has no apparent charge transfer. The charge transfer coefficient (and the Tafel slope) could be highly sensitive to the interface composition (e.g. the IS structure), which is related to the local surface electronic and geometrical structure and the solvent. Future studies based on DFT/CM-MPB method are necessary to quantify the Tafel kinetics at different surface sites.

As for the reaction rate, the calculated rate on Pt(111) surface is $8.9 \times 10^{-5}\ A/cm^2$ at ~0.4 V, which agrees reasonably with the experimental measurement. For example, Wieckowski et al. reported $\sim 10^{-5}\ A/cm^2$ on pc-Pt at about 0.45 V (methanol 0.6 M and 0.1 M H_2SO_4 solution) [23]; Housmans et al. reported $1.8 \times 10^{-6}\ A/cm^2$ on Pt(554) and Pt(553) at 0.4 V (methanol 0.025 M CH_3OH and 0.5 M H_2SO_4 solution) [11]. Considering that our calculations are performed on Pt(111), the consistency between theory and experiment should imply that C–H activation at the low potentials is not (so) sensitive to surface structure: The (111) terrace is active enough for the C – H bond breaking towards the CO formation. This could explain the observed small difference in activity (only 2 $\mu A/cm^{-2}$) between Pt(554), Pt(553) and Pt(111) [11] and the fact that the Pt catalyst can be rapidly poisoned due to CO formation in methanol oxidation [33,59].

4. Conclusion

This work represents a theoretical survey of the electrocataltyic methanol oxidation kinetics at the Pt(111)/water interface. By using the DFT method integrated with a periodic continuum solvation model based on the modified-Poisson–Boltzmann electrostatics, we resolve the potential-dependent kinetics of methanol decomposition on Pt(111) and deduce the charge transfer coefficient and Tafel slope from theory. We expect that the theoretical method and model utilized

here for methanol oxidation can be applied in general for understanding the electrocatalytic reactions of organic molecules at the solid–liquid interface. Our main results are outlined in the following.

(i) The free energy profiles of the C–H and O–H pathways are calculated, which shows that the C – H bond breaking is the kinetically preferred channel for methanol oxidation. The first C – H bond breaking is the rate-determining step and its free energy barrier is calculated to be 0.70 eV at 0.32 V vs. SHE. The preference of the C – H bond breaking over the O – H bond breaking could be explained by thermodynamics, where the adsorbed CH_2OH fragment is much more stable than the CH_3O fragment on the surface.

(ii) The first C – H bond breaking reaction does not involve apparent charge transfer and the reaction may be formally written as $CH_3OH(aq) \rightarrow CH_2OH^{*q+} + H^* + q^-$. The charge transfer coefficient is calculated to be 0.36, an unconventional value for charge transfer reaction, and the Tafel slope is deduced to be 166 mV.

(iii) Using microkinetics we calculated the current of methanol oxidation on Pt(111) as 8.9×10^{-5} A/cm^2 at ~ 0.4 V vs. SHE. The theoretical result is consistent with those reported in the experiment on various Pt catalysts, which indicates that Pt(111) is the active site for methanol oxidation towards CO formation.

Acknowledgments

This work is supported by NSFC (21173051, 21103110, 21361130019), 973 Program (2011CB808500, 2013CB83460), Science and Technology Commission of Shanghai Municipality (08DZ2270500), Innovation Program of Shanghai Municipal Education Commission (13YZ120), Program for Professor of Special Appointment (Eastern Scholar) at Shanghai Institute of Higher Learning, China and Shanghai Postdoctoral Science Foundation (2012 M520040, 2013 T60413, 12R21411200) for the financial support.

Appendix A. Supplementary data

Supplementary data to this article can be found online at http://dx.doi.org/10.1016/j.susc.2014.05.014.

References

[1] C. Lamy, A. Lima, V. LeRhun, F. Delime, C. Coutanceau, J.-M. Léger, J. Power. Sources 105 (2002) 283.
[2] N. Marković, P. Ross Jr., Surf. Sci. Rep. 45 (2002) 117.
[3] A. Arico, S. Srinivasan, V. Antonucci, Fuel Cells 1 (2001) 133.
[4] Y.X. Chen, A. Miki, S. Ye, H. Sakai, M. Osawa, J. Am. Chem. Soc. 125 (2003) 3680.
[5] P. Ferrin, A.U. Nilekar, J. Greeley, M. Mavrikakis, J. Rossmeisl, Surf. Sci. 602 (2008) 3424.
[6] M. Sevilla, C. Sanchís, T. Valdés-Solís, E. Morallón, A. Fuertes, Electrochim. Acta 54 (2009) 2234.
[7] H. Liu, C. Song, L. Zhang, J. Zhang, H. Wang, D.P. Wilkinson, J. Power. Sources 155 (2006) 95.
[8] R. Chetty, S. Kundu, W. Xia, M. Bron, W. Schuhmann, V. Chirila, W. Brandl, T. Reinecke, M. Muhler, Electrochim. Acta 54 (2009) 4208.
[9] A.N. Gavrilov, E.R. Savinova, P.A. Simonov, V.I. Zaikovskii, S.V. Cherepanova, G.A. Tsirlina, V.N. Parmon, Phys. Chem. Chem. Phys. 9 (2007) 5476.
[10] K. Kunimatsu, H. Hanawa, H. Uchida, M. Watanabe, J. Electroanal. Chem. 632 (2009) 109.
[11] T. Housmans, M. Koper, J. Phys. Chem. B 107 (2003) 8557.
[12] A.B. Anderson, E. Grantscharova, S. Seong, J. Electrochem. Soc. 143 (1996) 2075.
[13] H. Wang, C. Wingender, H. Baltruschat, M. Lopez, M. Reetz, J. Electroanal. Chem. 509 (2001) 163.
[14] H. Hoster, T. Iwasita, H. Baumgärtner, W. Vielstich, Phys. Chem. Chem. Phys. 3 (2001) 337.
[15] A. El-Shafei, R. Hoyer, L. Kibler, D. Kolb, J. Electrochem. Soc. 151 (2004) F141.
[16] N.M. Marković, H.A. Gasteiger, P.N. Ross Jr., X. Jiang, I. Villegas, M.J. Weaver, Electrochim. Acta 40 (1995) 91.
[17] R. Lampitt, L.L. Carrette, M. Hogarth, A. Russell, J. Electroanal. Chem. 460 (1999) 80.
[18] T. Iwasita, Electrochim. Acta 47 (2002) 3663.
[19] V. Radmilovic, H. Gasteiger, P. Ross, J. Catal. 154 (1995) 98.
[20] Y. Li, L. Tang, J. Li, Electrochem. Commun. 11 (2009) 846.
[21] S. Guo, S. Zhang, X. Sun, S. Sun, J. Am. Chem. Soc. 133 (2011) 15354.
[22] E. Herrero, W. Chrzanowski, A. Wieckowski, J. Phys. Chem. 99 (1995) 10423.
[23] G.Q. Lu, W. Chrzanowski, A. Wieckowski, J. Phys. Chem. B 104 (2000) 5566.
[24] S. Sriramulu, T. Jarvi, E. Stuve, J. Electroanal. Chem. 467 (1999) 132.
[25] E. Herrero, K. Franaszczuk, A. Wieckowski, J. Phys. Chem. 98 (1994) 5074.
[26] G. Tritsaris, J. Rossmeisl, J. Phys. Chem. C 116 (2012) 11980.
[27] J. Greeley, M. Mavrikakis, J. Am. Chem. Soc. 126 (2004) 3910.
[28] M. Neurock, M. Janik, A. Wieckowski, Faraday Discuss. 140 (2009) 363.
[29] P. Ferrin, M. Mavrikakis, J. Am. Chem. Soc. 131 (2009) 14381.
[30] S.K. Desai, M. Neurock, K. Kourtakis, J. Phys. Chem. B 106 (2002) 2559.
[31] J. Kua, W.A. Goddard, J. Am. Chem. Soc. 121 (1999) 10928.
[32] Y. Okamoto, O. Sugino, Y. Mochizuki, T. Ikeshoji, Y. Morikawa, Chem. Phys. Lett. 377 (2003) 236.
[33] S.X. Liu, L.W. Liao, Q. Tao, Y.X. Chen, S. Ye, Phys. Chem. Chem. Phys. 13 (2011) 9725.
[34] J. Greeley, M. Mavrikakis, J. Am. Chem. Soc. 124 (2002) 7193.
[35] Z.-P. Liu, S.J. Jenkins, D.A. King, Phys. Rev. Lett. 94 (2005) 196102.
[36] P. Liu, S.J. Jenkins, D.A. King, Phys. Rev. Lett. 93 (2004) 156102.
[37] Y.-H. Fang, G.-F. Wei, Z.-P. Liu, J. Phys. Chem. C 118 (2004) 3628.
[38] Y.F. Li, Z.P. Liu, L.L. Liu, W.G. Gao, J. Am. Chem. Soc. 132 (2010) 13008.
[39] H.F. Wang, Z.P. Liu, J. Phys. Chem. C 113 (2009) 17502.
[40] J.M. Soler, E. Artacho, J.D. Gale, A. Garcia, J. Junquera, P. Ordejon, D. Sanchez-Portal, J. Phys. Condens. Matter 14 (2002) 2745.
[41] J. Junquera, O. Paz, D. Sanchez-Portal, E. Artacho, Phys. Rev. B 64 (2001) 235111.
[42] N. Troullier, J.L. Martins, Phys. Rev. B 43 (1991) 1993.
[43] J.P. Perdew, K. Burke, M. Ernzerhof, Phys. Rev. Lett. 77 (1996) 3865.
[44] H.F. Wang, Z.P. Liu, J. Am. Chem. Soc. 130 (2008) 10996.
[45] C. Shang, Z.P. Liu, J. Chem. Theory Comput. 8 (2012) 2215.
[46] C. Shang, Z.P. Liu, J. Chem. Theory Comput. 6 (2010) 1136.
[47] Y.H. Fang, Z.P. Liu, J. Phys. Chem. C 114 (2010) 4057.
[48] Y.H. Fang, G.F. Wei, Z.P. Liu, Catal. Today 202 (2013) 98.
[49] C. Shang, Z.P. Liu, J. Am. Chem. Soc. 133 (2011) 9938.
[50] G.F. Wei, Y.H. Fang, Z.P. Liu, J. Phys. Chem. C 116 (2012) 12696.
[51] Y.H. Fang, G.F. Wei, Z.P. Liu, J. Phys. Chem. C 117 (2013) 7669.
[52] H. Ogasawara, B. Brena, D. Nordlund, M. Nyberg, A. Pelmenschikov, L. Pettersson, A. Nilsson, Phys. Rev. Lett. 89 (2002) 276102.
[53] P. Vassilev, R.A. van Santen, M.T.M. Koper, J. Chem. Phys. 122 (2005).
[54] D.R. LIDE (Ed.), CRC Handbook of Chemistry and Physics, CRC press, 2003-2004.
[55] Z.P. Liu, S.J. Jenkins, D.A. King, J. Am. Chem. Soc. 126 (2004) 10746.
[56] S. Trasatti, E. Lust, Modern Aspects of Electrochemistry, Kluwer Academic/Plenum Publishers, New York, Boston, Dordrecht, London, Moscow, 2002.
[57] D. Cao, G.Q. Lu, A. Wieckowski, S.A. Wasileski, M. Neurock, J. Phys. Chem. B 109 (2005) 11622.
[58] Y.H. Fang, Z.P. Liu, J. Am. Chem. Soc. 132 (2010) 18214.
[59] D. Kardash, J. Huang, C. Korzeniewski, Langmuir 16 (2000) 2019.